Monthly Notices of the ROYAL ASTRONOMICAL SOCIETY

MNRAS **448,** 2890–2899 (2015) doi:10.1093/mnras/stv147

Ultrashort-period main-sequence eclipsing systems: new observations and light-curve solutions of six NSVS binaries

Dinko P. Dimitrov[1]★ and Diana P. Kjurkchieva[2]

[1]*Institute of Astronomy, and NAO, Bulgarian Academy of Sciences, Tsarigradsko shossee 72, 1784 Sofia, Bulgaria*
[2]*Department of Physics, Shumen University, 9700 Shumen, Bulgaria*

Accepted 2015 January 19. Received 2015 January 12; in original form 2014 November 17

ABSTRACT

We carried out photometric and low-resolution spectral observations of six eclipsing ultrashort-period binaries with main-sequence (MS)components. The light-curve solutions of the Rozhen observations show that all targets are overcontact systems. We found a well-defined empirical relation between period and semi-major axis for the short-period binaries and used it for estimation of the global parameters of the targets. Our results revealed that NSVS 925605 is quite an interesting target: (i) it is one of a few contact binaries with M components; (ii) it exhibits high activity (emission in the Hα line, X-ray emission, large cool spots, non-Planck energy distribution); (iii) its components differ in temperature by 700 K. All the appearances of high magnetic activity and the huge fill-out factor (0.7) of NSVS 925605 may be a precursor of the predicted merging of close magnetic binaries. Another unusual binary is NSVS 2700153, which reveals considerable long-term variability.

Key words: binaries: eclipsing – stars: fundamental parameters – stars: individual: NSVS 925605 – stars: late-type.

1 INTRODUCTION

Short-period binaries with non-degenerate components are important objects in astrophysics, especially as regards understanding the very late evolutionary stages of the binaries connected with the processes of mass and angular momentum loss, merging or fusion of the stars, etc. However, their structure and evolution remain unsolved problems in stellar astrophysics, due to poor statistics. There are two reasons for this insufficiency.

First, the period distribution of binaries reveals a very sharp decline in the number of short-period systems below 0.27 d (Drake et al. 2014). Systems with periods around the short-period limit of 0.22 d (Rucinski 1992) are extremely rare: the fraction of ultrashort-period objects has been estimated at only 0.26 per cent of the total number of contact systems (Drake et al. 2014). Secondly, the faintness of late short binaries makes them difficult targets for detailed study. As a result, although M dwarfs form the most common stellar population in our Galaxy (∼70 per cent by number: Henry et al. 1999), their intrinsic faintness is a barrier to studying their binary characteristics.

Lately, a hypothesis has appeared: that very short period low-mass binaries could merge via 'magnetic braking' and, if a substantial amount of mass remains in orbit around the primary, it would form a disc in which planets could be produced, particularly hot Jupiters (Martin, Spruit & Tata 2011).

Fortunately, modern large stellar surveys during the last decade have allowed us to discover binaries with shorter and shorter periods (Maceroni & Rucinski 1997; Weldrake et al. 2004; Rucinski 2007; Pribulla et al. 2009; Dimitrov & Kjurkchieva 2010; Norton et al. 2011; Nefs et al. 2012; Davenport et al. 2013; Drake et al. 2014; Lohr et al. 2014; Qian et al. 2014, etc.).

This article presents our observations and light-curve solutions of six ultrashort-period binaries (with periods below 0.23 d).

2 SELECTION OF TARGETS

Using our own approach (Dimitrov 2009) to searching for stellar variability, we reviewed the Northern Sky Variability Survey (NSVS) data base (Woźniak et al. 2004) and found around 300 ultrashort-period candidates with W UMa type light curves. More than 100 of them were removed as probable δ Sct stars, due to their small infrared colours (temperatures $T > 6000$ K). We carried out short test observations of the remaining candidates and established that most of them were not variable stars. In such a way, we managed to separate a sample of about 40 ultrashort-period candidates from the NSVS survey appropriate for follow-up observations at Rozhen observatory ($\delta > -10^{\circ}$). Our study of one of them (BX Tri) has already been published (Dimitrov & Kjurkchieva 2010).

Table 1 reveals the coordinates and magnitudes of six other targets from this sample: four of them are newly discovered eclipsing stars, while two of them are identified with objects from the lists of ultrashort-period binaries of Norton et al. (2011) and Lohr et al.

★ E-mail: dinko@astro.bas.bg

Table 1. List of our ultrashort-period targets.

Target	NSVS ID	α [2000]	δ [2000]	R_{NSVS} [mag]	Period [d]	References
1	4484038	05 54 16.99	+44 25 34.1	12.50	0.2185	Norton et al. (2011)
2	7179685	06 46 06.47	+36 20 21.1	14.90	0.2097	New
3	4761821	08 01 50.03	+47 14 33.8	13.10	0.2175	Norton et al. (2011)
4	2700153	13 43 51.43	+63 04 22.8	12.48	0.2285	New
5	925605	14 01 46.37	+77 16 38.7	13.73	0.2176	New
6	8626028	21 16 26.81	+25 17 36.2	13.78	0.2174	New

Table 2. Journal of the Rozhen photometric observations.

Date	Filter	Exp. [s]	Number	Telescope
		NSVS 4484038		
2010 Feb 24	*VI*	120, 60	16, 16	60-cm
2010 Dec 08	*VI*	120, 60	90, 90	60-cm
2011 Jan 08	*VI*	120, 90	87, 86	60-cm
		NSVS 7179685		
2009 Sept 29	*R*	120	40	60-cm
2009 Sept 30	*R*	120	132	60-cm
2009 Oct 23	*VRI*	120, 120, 120	50, 50, 50	60-cm
2010 Mar 06	*R*	120	95	60-cm
2010 Mar 12	*I*	120	310	60-cm
2011 Jan 01	*V*	40	434	2-m
		NSVS 4761821		
2009 Nov 19	*R*	120	50	60-cm
2011 Jan 01	*VI*	120, 60	103, 103	60-cm
2011 Jan 06	*VI*	120, 120	85, 85	60-cm
2011 Jan 13	*VI*	120, 120	18, 16	60-cm
		NSVS 2700153		
2010 May 16	*VI*	120, 120	8, 20	60-cm
2010 June 20	*VI*	120, 120	86, 85	60-cm
2010 Nov 21	*VI*	120, 120	21, 21	60-cm
2011 Jan 17	*VI*	120, 120	82, 82	Shmidt
2011 Jan 18	*V*	120	125	Shmidt
2011 Jan 19	*I*	120	155	Shmidt
		NSVS 925605		
2009 June 05	*R*	120	100	60-cm
2009 June 06	*R*	120	100	60-cm
2009 July 27	*V*	120	91	60-cm
2009 Aug 26	*VRI*	120, 60, 60	50, 50, 50	60-cm
2009 Aug 27	*VRI*	120, 60, 60	60, 60, 60	60-cm
		NSVS 8626028		
2009 Aug 26	*VRI*	120, 60, 60	50, 50, 50	60-cm
2009 Aug 27	*VRI*	120, 60, 60	59, 60, 60	60-cm

(2014), based on the SuperWide Angle Search for Planets (SuperWASP) photometric survey (Pollacco et al. 2006).

Besides photometric data for all six targets in the NSVS data base, we also found data for four of them in the SuperWASP archive (Butters et al. 2010). Periodogram analysis of these low-precision but numerous data allowed us to determine their ephemeris (Table 1). Fig. A1 in the Appendix presents the folded curves of the targets corresponding to their old photometric data.

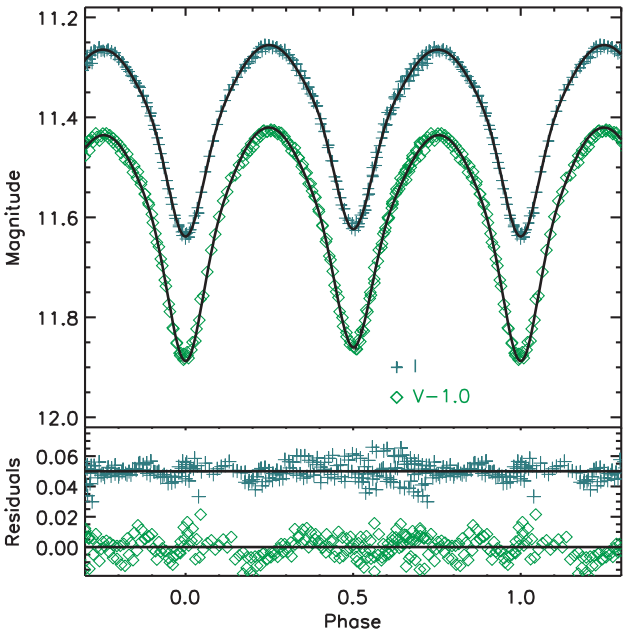

Figure 1. Top: folded light curves of NSVS 4484038 and their fits (continuous lines). Bottom: the corresponding residuals. The photometric data in some filters are shifted vertically by a different number for better visibility. A colour version of this figure is available in the online journal.

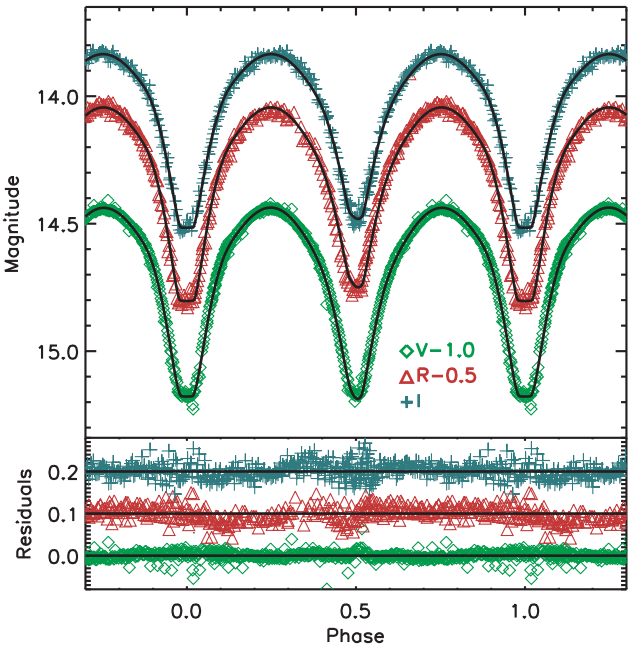

Figure 2. Same as Fig. 1, for NSVS 7179685.

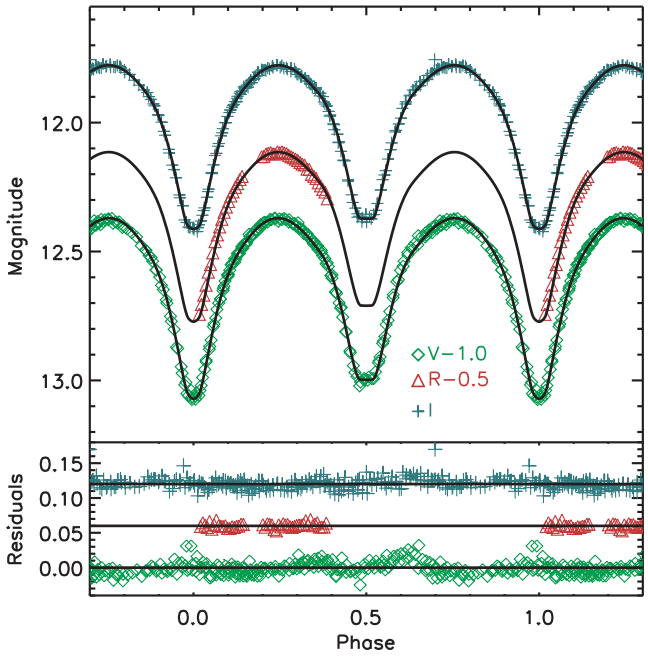

Figure 3. Same as Fig. 1, for NSVS 4761821.

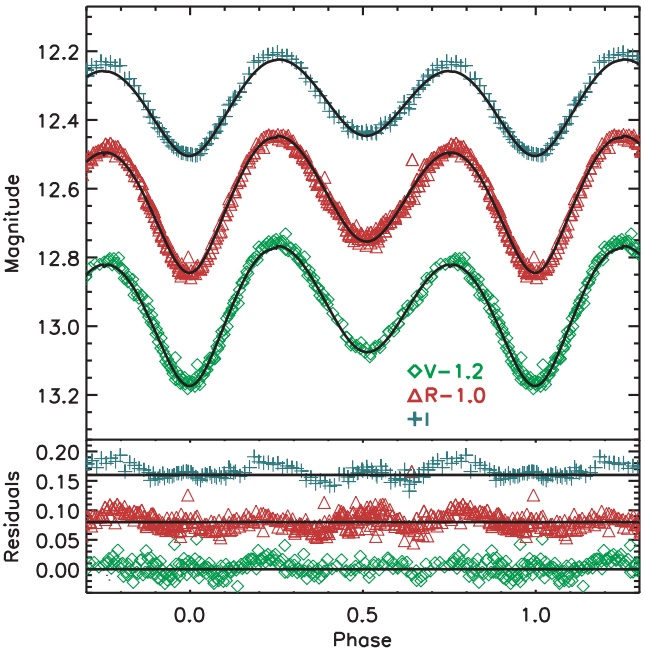

Figure 5. Same as Fig. 1, for NSVS 925605.

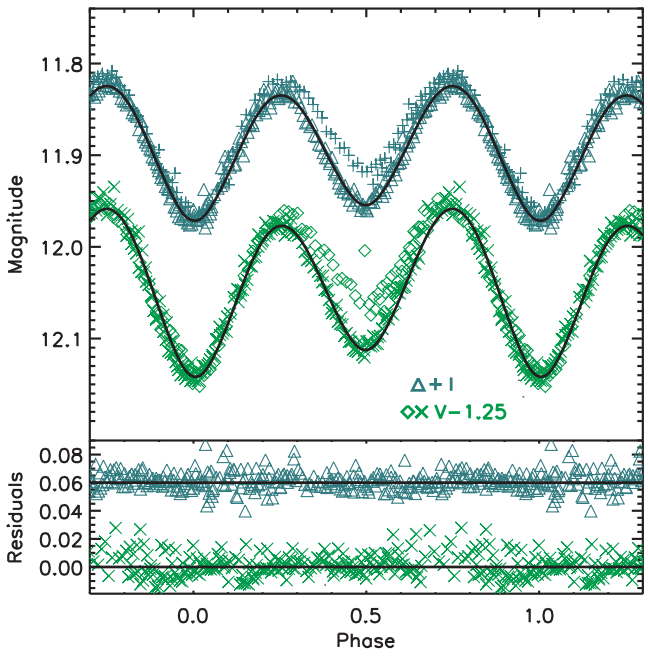

Figure 4. Same as Fig. 1, for NSVS 2700153.

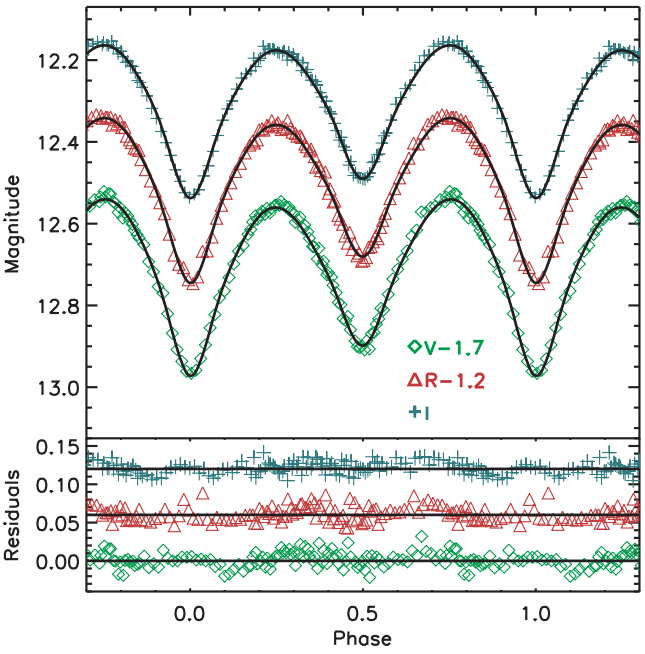

Figure 6. Same as Fig. 1, for NSVS 8626028.

3 ROZHEN OBSERVATIONS AND DATA REDUCTION

Follow-up CCD photometry of the targets in the *VRI* bands was carried out with the three telescopes of the Rozhen National Astronomical Observatory (Table 2). The 2-m RCC telescope is equipped with a VersArray CCD camera (1340 × 1300 pixels, 20 μm pixel^{-1}, field of 5.35 × 5.25 arcmin^2). The 60-cm Cassegrain telescope is equipped with a FLI PL09000 CCD camera (3056 × 3056 pixels, 12 μm pixel^{-1}, field of 17.1 × 17.1 arcmin^2). The 50/70 cm Schmidt telescope has a field of view (FoV) of around 1° and is equipped with a FLI PL 16803 CCD camera, 4096 × 4096 pixels, 9 μm pixel^{-1} size.

Standard stars of Landolt (1992) and standard fields of Stetson (2000) were used for transition from the instrumental system to a standard photometric system.

Standard Interactive Data Language procedures (adapted from DAOPHOT) were used for reduction of the photometric data. More than five standard stars were chosen in the observed fields of each target, using the requirement of being constant within 0.015 mag during all observational runs and in all filters. Table A1 in the Appendix presents their V, $B-V$, $V-R$ and $V-I$ determined by our observations (for the targets, they correspond to phase 0.25), as

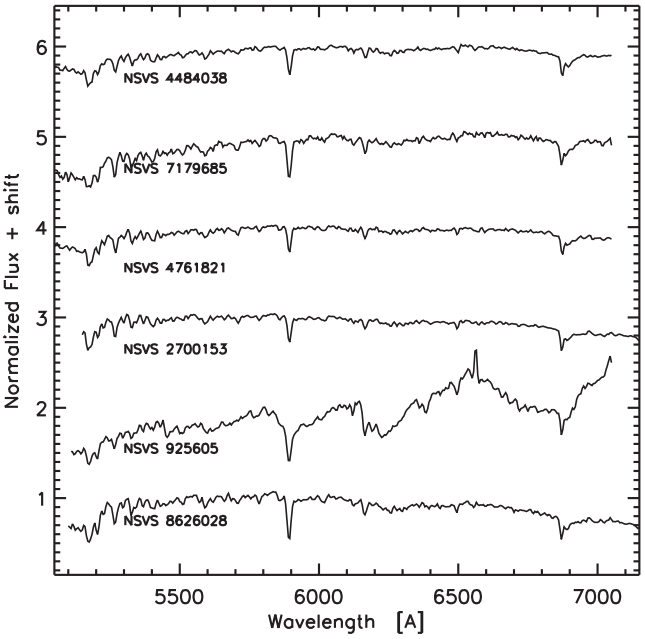

Figure 7. The low-resolution spectra of the targets around the Hα line.

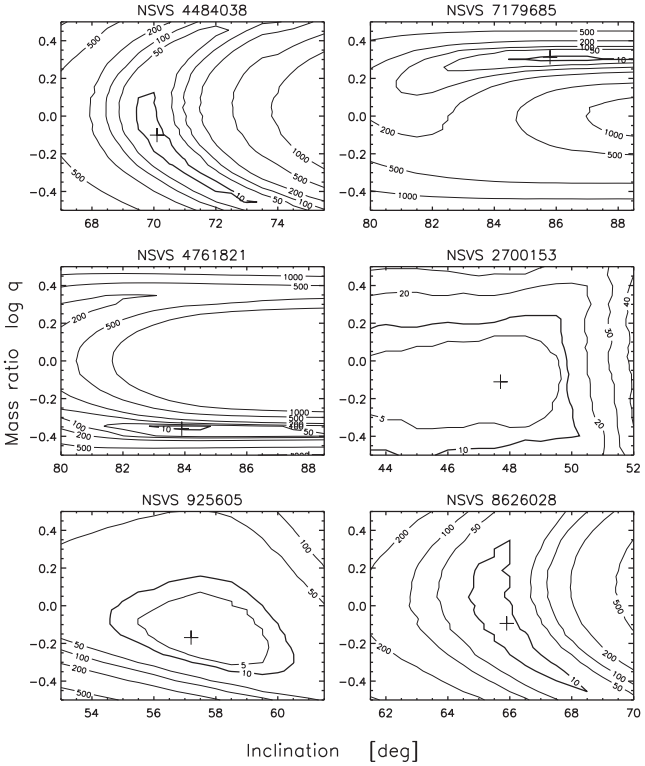

Figure 8. Diagrams of i, $\log q$ with isolines corresponding to different values of normalized χ^2; '+' symbols mark the positions of $\chi^2_{\rm min}$(abs).

well as their $J-K$ colours from the 2MASS catalogue (Skrutskie et al. 2006).

Figs 1–6 present the follow-up Rozhen photometry of our targets. Table A2 presents a sample of the Rozhen photometric data (the full table is available in the online version of the article; see Supporting Information).

We calculated the times of observed light minima by the method described in Pribulla et al. (2012). Table A3 contains their *HJD*(Min), epoch and $O-C$.

We obtained low-resolution spectra (Fig. 7) over five nights during 2011 February–May, using the 2-m RCC telescope equipped with focal reducer FoReRo-2. We used a grism with 300 line mm^{-1}, which allows a resolution of 5.223 Å pixel^{-1} in the range 5000–7000 Å. These low-resolution spectra do not allow radial velocity measurements but are useful indicators of the temperature and stellar activity.

4 LIGHT-CURVE SOLUTIONS

The photometric data (Figs 1–6) implied that our targets are contact or overcontact systems, as was expected from their ultrashort orbital periods.

We carried out modelling of the Rozhen photometric data using the code PHOEBE (Prša & Zwitter 2005), using the following procedure.

We determined in advance the mean temperatures $T_{\rm m}$ of the binaries (Table 3), using their infrared colour indices $(J-K)$ from the 2MASS catalogue and the colour–temperature calibration of Tokunaga (2000). The 'spectral' temperatures of the targets, obtained by comparison of their low-resolution spectra (Fig. 7) with those of standard stars with known temperatures, were almost the same as the values of $T_{\rm m}$ in Table 3.

First, we assumed $T_1^0 = T_{\rm m}$ and searched for solutions for fixed T_1^0 and $q^0 = 1$, varying the ephemeris, secondary temperature T_2, orbital inclination i and potentials $\Omega_{1,2}$.

We adopted coefficients of 0.32 for gravity-brightening and 0.5 for reflection, appropriate for late stars. The linear limb-darkening coefficients were interpolated from the values of Van Hamme (1993). In order to reproduce the O'Connell effect, we added cool spots on the components and varied their parameters: longitude β, latitude λ, angular size α and temperature factor $k = T_{\rm sp}/T_1$. To obtain a good fit in all colours, a third light was necessary for some targets.

As a result of the first stage of the light-curve solution, we obtained initial values T_2^0, i^0 and $\Omega_{1,2}^0$, as well as the ephemeris and spot parameters for each target. Further, we determined the mass ratio by applying the *q-search* method. We calculated the normalized χ^2 for a two-dimensional grid (i, $\log q$), consisting of values of i within the 10° range around the value i° with step 0.5° and q values 0.15, 0.20, ..., 0.95, 1.00, 1/0.95, 1/0.90, ..., 1/0.20, 1/0.15 (T_1^0, T_2^0 and spot parameters were fixed). In this way, we obtained $\chi^2_{\rm min}(1)$, corresponding to the first approximation (i^1, q^1). This procedure was repeated around the pair (i^1, q^1) for a finer grid, corresponding to a ten times smaller q step and five times smaller i step. The $\chi^2_{\rm min}(2)$ obtained corresponded to the second

Table 3. The 2MASS colour indices $J-K$ and corresponding mean temperatures $T_{\rm m}$ of the targets.

Target	NSVS 4484038	NSVS 7179685	NSVS 4761821	NSVS 2700153	NSVS 925605	NSVS 8626028
$J-K$	0.590 ± 0.030	0.798 ± 0.033	0.651 ± 0.033	0.635 ± 0.037	0.863 ± 0.028	0.769 ± 0.028
$T_{\rm m}$	4950 ± 150	4040 ± 190	4690 ± 130	4730 ± 200	3490 ± 250	4200 ± 180

Table 4. Results from the light-curve solutions.

Parameter		NSVS 4484038	NSVS 7179685	NSVS 4761821	NSVS 2700153	NSVS 925605	NSVS 8626028
P	[d]	0.218493	0.209740	0.217513	0.228456	0.217629	0.217407
		±0.000001	±0.000001	±0.000001	±0.000001	±0.000001	±0.000001
HJD_0	[d]	5539.479711	5104.528662	5563.438743	5368.312230	4988.575181	5070.408406
+245 0000		±0.000035	±0.000011	±0.000020	±0.000114	±0.000028	±0.000051
i	[°]	70.1	85.5	83.8	47.8	57.2	65.9
		±0.1	±0.2	±0.1	±0.4	±0.2	±0.1
$q = M_2/M_1$		0.792	2.128	0.432	0.775	0.678	0.805
		±0.002	±0.007	±0.001	±0.003	±0.003	±0.002
T_1	[K]	5000	4100	4685	4785	3813	4318
		±43	±32	±32	±51	±51	±27
T_2	[K]	4897	3979	4696	4689	3135	4095
		±41	±29	±29	±40	±65	±22
r_1		0.407	0.326	0.464	0.409	0.474	0.418
r_2		0.364	0.456	0.318	0.364	0.408	0.380
l_2/l_1		0.727	1.731	0.479	0.709	0.221	0.592
$\Omega_1 = \Omega_2$		3.365	5.316	2.707	3.343	2.930	3.330
		±0.004	±0.006	±0.006	±0.007	±0.010	±0.004
FF		0.0857	0.193	0.136	0.071	0.702	0.207
Spot_1		primary	primary	–	–	primary	primary
λ	[°]	115	270	–	–	115	225
β	[°]	90	90	–	–	63	70
α	[°]	13	15	–	–	16	9
κ		0.9	0.9	–	–	0.84	0.9
Spot_2		–	–	–	–	secondary	primary
λ	[°]	–	–	–	–	178	310
β	[°]	–	–	–	–	90	90
α	[°]	–	–	–	–	18	11
T_{Spot2}	[K]	–	–	–	–	0.8	0.9
$l_3(V)$		0.015	0.012	0.014	–	0.089	0.036
		±0.004	±0.003	±0.010	–	±0.012	±0.011
$l_3(R)$		–	–	–	–	0.078	0.048
		–	–	–	–	±0.010	±0.009
$l_3(I)$		0.112	0.007	–	0.069	0.293	0.056
		±0.003	±0.004	–	±0.008	±0.011	±0.005

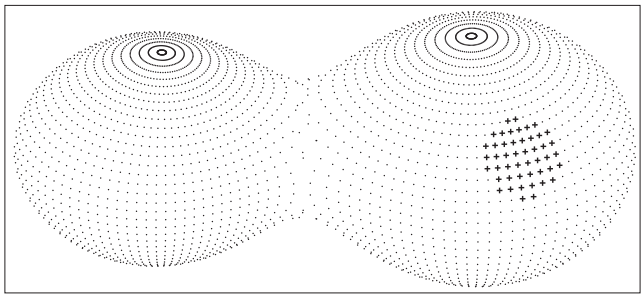

Figure 9. 3D configuration of the strongly overcontact target NSVS 925605.

approximation (i^2, q^2), etc. Thus we reach the absolute minimum with $\chi^2_{\mathrm{min}}(\mathrm{abs}) \sim 1$, corresponding to the final values (i^{f}, q^{f}).

The (i, log q) diagrams show that the solution ambiguity increases rapidly with decreasing orbital inclination (Fig. 8). Maceroni, Milano & Russo (1985) reached the same result by another procedure.

We searched for the best fit for fixed i^{f}, q^{f}, ephemerides and spot parameters, varying T_2, $\Omega_{1,2}$ and the third light $l_3(V, R, I)$. Finally, we calculated T_1 and T_2. To this aim, we developed the approach of Coughlin et al. (2011):

$$T_1 = T_{\mathrm{m}} + \frac{\Delta T}{c+1}, \tag{1}$$

$$T_2 = T_1 - \Delta T, \tag{2}$$

where $c = l_2/l_1$ and ΔT (difference of temperatures of the components) are determined from the PHOEBE solution.

Table 4 contains the final values of all parameters determined: period P; initial epoch HJD_0; orbital inclination i; temperatures of the components $T_{1,2}$; potentials of the components $\Omega_{1,2}$; fill-out factor FF; spot parameters; third-light contribution in the different colours $l_3(V, R, I)$. The errors in the parameters in Table 4 are the formal PHOEBE values.

The synthetic light curves corresponding to the parameters from Table 4 are shown in Figs 1–6 as continuous lines.

The mass ratio parameter deserves special attention. Although its determination through analysis of the light curve is an ambiguous approach, compared with that using a radial velocity solution, the rapid rotation of the components of ultrashort-period binaries is a serious obstacle to obtaining a precise spectral mass ratio from measurement of their highly broadened and blended spectral lines (Bilir et al. 2005; Dall & Schmidtobreick 2005). In contrast, tests have revealed that photometric mass ratios are more reliable than spectroscopic ones for totally eclipsing W UMa type stars and are sufficiently reliable for partially eclipsing systems (Maceroni & van't Veer 1996), because their eclipse depths depend strongly on the geometrical parameters and the mass ratio q. Hence, the

Table 5. Semi-major axes of short-period binaries from spectral studies.

Star	$P_{\rm orb}$	$M_1 + M_2$	a	References
CSS J090826.3+123648*	0.1392	0.80	1.049	Drake et al. (2014)
CSS J111647.8+294602*	0.1462	0.75	1.061	Drake et al. (2014)
CSS J081158.6+311959*	0.1562	0.70	1.083	Drake et al. (2014)
CSS J001242.4+130809*	0.1641	0.80	1.171	Drake et al. (2014)
CSS J001242.4+130809	0.1641	0.41	0.937	Drake et al. (2014)
CSS J090119.2+114254*	0.1867	0.70	1.222	Drake et al. (2014)
BX Tri	0.1926	0.77 ± 0.03	1.284 ± 0.022	Dimitrov & Kjurkchieva (2010)
BW3 V38	0.1984	0.85 ± 0.11	1.356 ± 0.085	Maceroni & Montalban (2004)
SDSS J001641-000925	0.1986	0.88 ± 0.08	1.372 ± 0.057	Davenport et al. (2013)
GSC 1387-475	0.2178	0.94 ± 0.03	1.492 ± 0.019	Rucinski & Pribulla (2008)
CC Com	0.2211	1.09 ± 0.02	1.585 ± 0.011	Pribulla et al. (2007)
1SWASP J160156.04+202821.6	0.2265	1.43 ± 0.06	1.761 ± 0.033	Lohr et al. (2014)
V523 Cas	0.2337	1.13 ± 0.04	1.663 ± 0.025	Rucinski et al. (2003)
RW Com	0.2373	1.18 ± 0.03	1.704 ± 0.060	Pribulla et al. (2009)
BI Vul	0.2518	1.45	1.899	Maceroni & van't Veer (1996)
1SWASP J150822.80-054236.9	0.2601	1.62 ± 0.10	2.013 ± 0.065	Lohr et al. (2014)
VZ Psc	0.2612	1.46 ± 0.06	1.950 ± 0.040	Hrivnak, Guinan & Lu (1995)
V803 Aql	0.2634	1.58	2.014	Maceroni & van't Veer (1996)
FS Cra	0.2636	1.51	1.984	Maceroni & van't Veer (1996)
44 Boo=i Boo	0.2678	1.47	1.987	Lu, Rucinski & Ogloza (2001)

Note: Stars with WD+dM models are marked with asterisks.

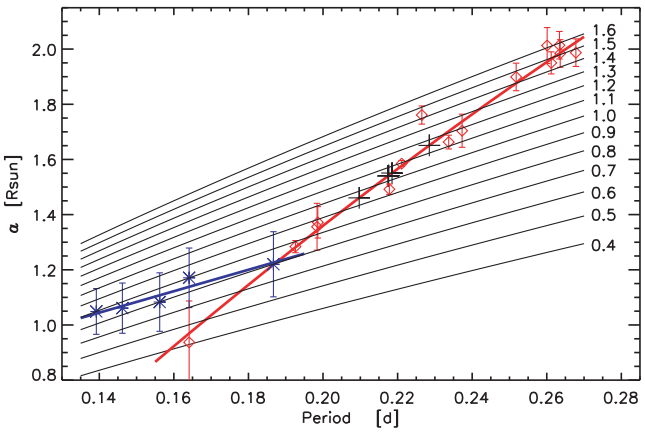

Figure 10. Period–semi-major axis diagram for short-period binaries. The thin black lines represent the isolines of binary (total) mass. The positions of the stars from Table 6 are marked by red diamonds, while those of our targets are marked by black plus symbols. The red line exhibits the empirical relation described by equation (3). The blue line presents the empirical relation for WD+dM binaries, marked with blue asterisks.

obtained photometric q values of our targets may be considered with confidence.

5 ANALYSIS OF THE RESULTS

The analysis of the light-curve solutions led us to several conclusions.

(i) All targets are overcontact (OC) binaries. The fill-out factor of NSVS 925605 is huge (Fig. 9).

(ii) The mass ratios of four targets are within the narrow range 0.68–0.8, while NSVS 7179685 and NSVS 4761821 have components which masses differ by a factor of 2. These two targets undergo total eclipses and correspondingly, their photometric mass ratios are more precise.

(iii) The differences between the temperatures of the components of the targets are up to 220 K, as expected for overcontact systems. The only exception is NSVS 925605, in which the cool components differ by nearly 700 K (although there is a large fill-out factor).

(iv) NSVS 7179685 is the only target in which the more massive star is the cooler component. We do not know any overcontact binaries with orbital period below 0.21 d with such a property.

(v) NSVS 925605 is a rare case of an overcontact ultrashort-period binary consisting of M dwarfs.

(vi) NSVS 2700153 revealed considerable long-term variability during our observations (Fig. 4): the secondary minimum was shallower than the primary one in 2010 June, but they became almost equal in depth in 2011 January. The parameters in Table 4 correspond to the light-curve solution from 2011 January.

(vii) NSVS 925605 shows high activity: emission in the Hα line (Fig. 7) from its chromosphere; X-ray emission from the corona (it is the only X-ray source among our six targets, identified as 1RXS J140139.8+771643); a large cool photospheric spot. The considerable contribution of third light, especially in the I colour (Table 4), cannot be explained by blurring because there is no nearby star within 1 arcsec of this target. The reason could be a non-Planck distribution of its energy. All the appearances of high magnetic activity and the huge fill-out factor of NSVS 925605 might be interpreted in light of the hypothesis of Martin et al. (2011) as a precursor of the merging of close magnetic binaries.

6 GLOBAL PARAMETERS OF THE TARGETS

Due to a lack of radial velocity curve solutions, we had to use empirical relations for determination of the global characteristics of our targets. With this aim, we built a period–semi-major axis (P, a) diagram on the basis of 14 binaries with $P < 0.27$ d that have a radial velocity solution and a modern light-curve solution (Table 5). Their distribution was approximated by a parabola:

$$a = -1.154 + 14.633 \times P - 10.319 \times P^2 \quad [\mathrm{R}_\odot], \qquad (3)$$

Table 6. Global parameters of the targets.

Name	a	R_1 R_2	M	M_1 M_2	L_1 L_2	M_{bol} M_V	d	J_{orb}
NSVS 4484038	1.55	0.63 ± 0.02	1.01	0.56 ± 0.06	0.23 ± 0.02	5.73 ± 0.11	200	0.151
	± 0.05	0.57 ± 0.02	± 0.10	0.45 ± 0.04	0.17 ± 0.02	5.928	± 12	± 0.034
NSVS 7179685	1.461	0.48 ± 0.02	0.95	0.30 ± 0.03	0.06 ± 0.01	6.68 ± 0.13	428	0.118
	± 0.05	0.67 ± 0.02	± 0.09	0.65 ± 0.06	0.10 ± 0.01	7.284	± 26	± 0.027
NSVS 4761821	1.541	0.71 ± 0.02	1.04	0.72 ± 0.07	0.23 ± 0.02	6.00 ± 0.10	248	0.137
	± 0.05	0.49 ± 0.02	± 0.10	0.32 ± 0.03	0.11 ± 0.01	6.397	± 12	± 0.030
NSVS 2700153	1.650	0.67 ± 0.02	1.15	0.65 ± 0.06	0.22 ± 0.02	5.81 ± 0.11	267	0.190
	± 0.05	0.60 ± 0.02	± 0.11	0.50 ± 0.05	0.16 ± 0.02	6.060	± 14	± 0.042
NSVS 925605	1.542	0.73 ± 0.02	1.04	0.62 ± 0.06	0.11 ± 0.01	6.82 ± 0.12	154	0.155
	± 0.05	0.64 ± 0.02	± 0.10	0.42 ± 0.04	0.024 ± 0.005	8.020	± 9	± 0.034
NSVS 8626028	1.540	0.63 ± 0.02	1.04	0.57 ± 0.06	0.13 ± 0.01	6.40 ± 0.10	184	0.159
	± 0.05	0.57 ± 0.02	± 0.10	0.47 ± 0.04	0.09 ± 0.01	7.904	± 9	± 0.035

where a is in solar radii and P in days. The standard deviation of the fit is 0.05 $R_\odot$ and we assume this value as a mean error in a for our targets with periods around 0.22 d.

Such a relation is expected for contact and overcontact binaries of MS late stars, for which $R_1 + R_2 \approx a$ and $R \sim M^k$, where $k \approx 1$. Then the third Kepler law leads to $a \sim P$, which is similar to the almost linear dependence (3) for periods of about 0.22 d (Fig. 10).

The (P, a) relation (3) corresponds to the following 'period–mass' relation for short-period binaries:

$$M = \frac{0.0134}{P^2}\left(-1.154 + 14.633 \times P - 10.319 \times P^2\right)^3 \ [M_\odot], \quad (4)$$

where M is the total mass of the binary.

It is important to know if there is a lower limit on the period–axis relation (3). Very recently, Drake et al. (2014) modelled binaries with extremely short periods using configurations consisting of a white dwarf and a dM star. They are stable non-accreting WD+MS systems, in contrast to the accretion-induced variability in CV variables. We added these five systems (Table 5) to our (P, a) diagram. It is interesting that their semi-axes and respective masses are almost the same (within the errors), while the orbital periods are quite different. The WD+dM models (blue asterisk) of four of these binaries fall away from the line approximating the (P, a) relation of binaries with MS components (red line). It can be seen that the dependence of the semi-axis of these extremely short-period binaries on the period (blue continuous line) is considerably weaker. One of them, CSS J001242.4+130809, has two models: WD+dM and dM+dM (Table 5). Its dM+dM model, as well as that of the longest-period target, CSS J090119.2+114254, falls just on the period–axis line of our MS binaries (Fig. 10). This may imply that such configurations are more appropriate for these two targets. Low-resolution spectroscopy of extremely short-period binaries (Drake et al. 2014) revealed the presence of Balmer emission and Ca H+K emission typical for late dwarfs and strong local magnetic fields.

We used the empirical relation (3) to obtain the semi-major axes a of our targets and also the following: masses $M_{1,2}$, radii $R_{1,2}$ and luminosities $L_{1,2}$ of their components in solar units; bolometric and visual absolute magnitudes M_{bol} and M_V of the targets; distance d in pc and orbital angular momenta J_{orb} (by the expression of Popper & Ulrich 1977). Table 6 contains the values of the global parameters obtained.

The orbital angular momenta of the targets (Table 6) are considerably smaller than those of the RS CVn binaries and detached systems, which have $\log J_{orb} \geq +0.08$. They are also smaller than those of ordinary contact systems, which have $\log J_{orb} \geq -0.5$. The J_{orb} values obtained are bigger only than those of the shortest-period CVs of SU UMa type.

7 CONCLUSIONS

We found a well-defined empirical relation between period and semi-major axis for short-period binaries and used it for estimation of the global parameters of six ultrashort-period targets.

One of them, NSVS 925605, with a huge fill-out factor and other peculiar characteristics (consisting of M components with high activity and a non-Planck energy distribution), is probably at the stage of merging.

Our results revealed that all six ultrashort-period targets with periods 0.20–0.23 d are overcontact systems. At the same time, the short-period binaries BX Tri and BW3 V38, with periods below 0.20, have detached configurations. Nefs et al. (2012) confirmed spectroscopically another detached system with 0.18 d period containing an M dwarf. It is worth studying which parameters determine the stellar configuration (detached, contact or overcontact) of ultrashort-period binaries.

ACKNOWLEDGEMENTS

The authors gratefully acknowledge observing grant support from the Institute of Astronomy and Rozhen National Astronomical Observatory, Bulgarian Academy of Sciences. The research was partly supported by funds of project RD-08-244 of Shumen University.

This research makes use of the SIMBAD, Vizier, and Aladin data bases, operated at CDS, Strasbourg, France, and NASA's Astrophysics Data System Abstract Service. This publication makes use of data products from the Two Micron All Sky Survey, which is a joint project of the University of Massachusetts and the Infrared Processing and Analysis Center/California Institute of Technology, funded by the National Aeronautics and Space Administration and the National Science Foundation. This research also has made use of the USNOFS Image and Catalogue Archive operated by the United States Naval Observatory, Flagstaff Station (http://www.nofs.navy.mil/data/fchpix/).

This research was based on data obtained with the telescopes at Rozhen National Astronomical Observatory, the Northern Sky Variability Survey (http://skydot.lanl.gov/nsvs/nsvs.php) and SuperWASP Public Archive first public data release DR1 (http://www.wasp.le.ac.uk/public/). The authors are grateful to an anonymous referee for valuable notes and propositions.

REFERENCES

Bilir S., Karatas Y., Demircan O., Eker Z., 2005, MNRAS, 357, 497
Butters O. W. et al., 2010, A&A, 520L, 10
Coughlin J. L., Lo'pez-Morales M., Harrison T. E., Ule N., Hoffman D. I., 2011, AJ, 141, 78
Dall T., Schmidtobreick L., 2005, A&A, 429, 625
Davenport J. R. A. et al., 2013, ApJ, 764, 62
Dimitrov D. P., 2009, Bulg. Astron. J., 12, 49
Dimitrov D. P., Kjurkchieva D. P., 2010, MNRAS, 406, 2559
Drake A. J. et al., 2014, ApJ, 790, 157
Henry T. J., Franz O. G., Wasserman L. H., Benedict G. F., Shelus P. J., Ianna P. A., Kirkpatrick J. D., McCarthy D. W. Jr., 1999, ApJ, 512, 864
Hrivnak B. J., Guinan E. F., Lu W., 1995, ApJ, 455, 300
Landolt A., 1992, AJ, 104, 340
Lohr M. E., Hodgkin S. T., Norton A. J., Kolb U. C., 2014, A&A, 563A, 34
Lu W., Rucinski S. M., Ogloza W., 2001, AJ, 122, 402
Maceroni C., Montalban J., 2004, A&A, 426, 577
Maceroni C., Rucinski S. M., 1997, PASP, 109, 782
Maceroni C., van't Veer F., 1996, A&A, 311, 523
Maceroni C., Milano L., Russo G., 1985, MNRAS, 217, 843
Martin E. L., Spruit H. C., Tata R., 2011, A&A, 535, 50
Nefs S. V. et al., 2012, MNRAS, 425, 950
Norton A. J. et al., 2011, A&A, 528A, 90
Pollacco D. L. et al., 2006, PASP, 118, 1407
Popper D., Ulrich R., 1977, ApJ, 212, L131
Pribulla T., Rucinski S. M., Conidis G., DeBond H., Thomson J. R., Gazeas K., Ogloza W., 2007, AJ, 133, 1977
Pribulla T. et al., 2009, AJ, 137, 3646
Pribulla T. et al., 2012, Astron. Nachr., 333, 754
Prša A., Zwitter T., 2005, ApJ, 628, 426
Qian S.-B., Jiang L.-Q., Zhu L.-Y., Zejda M., Mikulášek Z., Fernández-Lajús E., Liu N.-P., 2014, Contri. Astron. Obs. Skalnaté Pleso, 43, 290
Rucinski S. M., 1992, AJ, 103, 960
Rucinski S. M., 2007, MNRAS, 382, 393
Rucinski S. M., Pribulla T., 2008, MNRAS, 388, 1831
Rucinski S. M. et al., 2003, AJ, 125, 3258
Skrutskie M. F. et al., 2006, AJ, 131, 1163
Stetson P., 2000, PASP, 112, 925
Tokunaga A. T., 2000, in Cox A. N., ed., Allen's Astrophysical Quantities, 4th edn. AIP Press, New York, p. 143
Van Hamme W., 1993, AJ, 106, 2096
Weldrake D. T. F., Sackett P. D., Bridges T. J., Freeman K. C., 2004, AJ, 128, 736
Woźniak P. R. et al., 2004, AJ, 127, 2436

APPENDIX A: ADDITIONAL INFORMATION

Fig. A1 presents the folded curves of the targets corresponding to their old photometric data.

Table A1 presents their V, $B-V$, $V-R$ and $V-I$ determined by our observations (for the targets, these correspond to phase 0.25), as well as their $J-K$ colours from the 2MASS catalogue. Table A2 presents a sample of the Rozhen photometric data (the full table is available in the online version of the article; see Supporting Information). Table A3 contains *HJD*(Min), epoch and $O-C$ values for our targets.

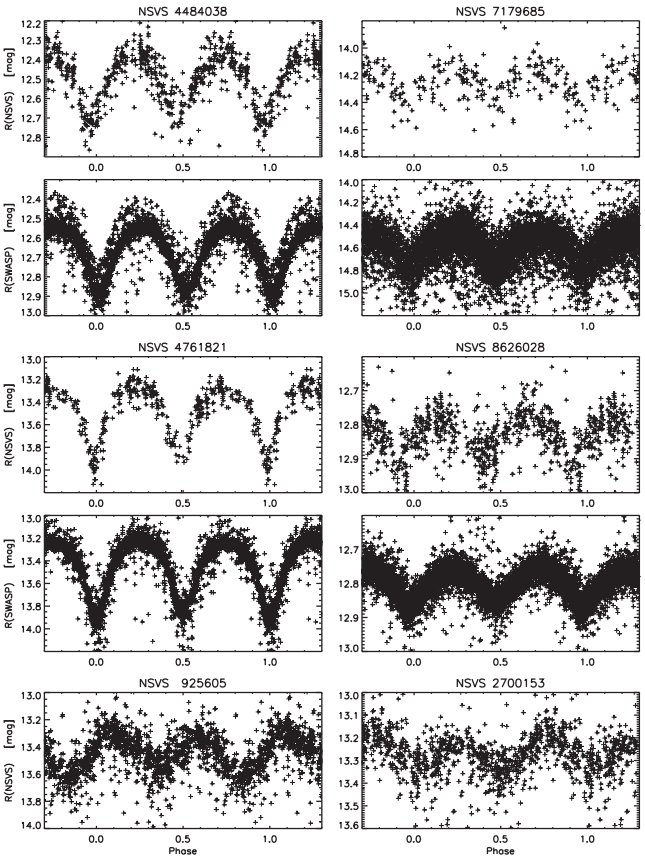

Figure A1. Folded light curves based on the NSVS and Super WASP observations of the targets.

Table A1. Colours of the targets and their standard stars.

Star	ID GSC1.2(2.3)	V [mag]	$B-V$ [mag]	$V-R$ [mag]	$V-I$ [mag]	$J-K$ [mag]
	NSVS 4484038					
Var	2924-0179	12.43	0.71	0.25	1.17	0.59
St1	2924-2161	12.86	1.00	0.40	1.31	0.69
St2	2924-1407	12.68	1.23	0.70	1.93	1.08
St3	2924-1435	13.23	0.60	0.16	0.78	0.37
St4	2924-0641	12.02	1.87	0.68	1.88	1.07
St5	2924-1202	11.79	0.86	0.13	0.69	0.34
St6	2924-1060	12.94	0.97	0.46	1.40	0.75
	NSVS 7179685					
Var	N8BM016247	15.44	0.45	0.91	1.61	0.80
St1	2448-0250	13.42	0.65	0.71	1.20	0.63
St2	N8BN012958	13.63	0.35	0.48	0.77	0.34
St3	2448-0995	13.29	1.34	0.77	1.42	0.74
St4*	N8BM016279	15.19	0.46	0.72	1.23	0.64
St5*	N8BM016265	15.64	0.28	0.71	1.29	0.69
St6*	N8BM016250	15.38	−0.20	0.43	0.69	0.24
St7*	N8BM016262	15.20	0.08	0.55	0.96	0.48
St8*	N8BM016256	15.82	0.10	0.55	0.95	0.44

Table A1 – *continued*.

Star	ID GSC1.2(2.3)	V [mag]	$B-V$ [mag]	$V-R$ [mag]	$V-I$ [mag]	$J-K$ [mag]
	NSVS 4761821					
Var	3408-0735	13.37	1.06	0.76	1.60	0.65
St1	3408-1475	11.58	0.82	0.74	1.44	0.49
St2	3408-0617	13.51	0.66	0.61	1.15	0.33
St3	3408-0431	12.59	0.69	0.83	1.72	0.74
St4	3408-0459	13.26	0.54	0.63	1.14	0.30
St5	3408-2017	13.54	0.73	0.66	1.18	0.31
	NSVS 2700153					
Var	4174-0776	13.19	0.82	0.71	1.37	0.64
St1	4174-1064	12.42	0.71	0.39	1.00	0.43
St2	4174-0970	12.99	0.68	0.42	0.95	0.43
St3	4174-0772	13.29	0.42	0.41	0.83	0.30
St4	4174-0696	12.07	0.53	0.43	0.83	0.31
St5	4174-0764	13.76	0.35	0.46	0.96	0.41
St6	4174-0526	14.03	0.46	0.37	1.02	0.46
	NSVS 925605					
Var	4558-0304	13.96	1.00	0.52	1.75	0.86
St1	4558-0096	14.09	0.19	−0.11	0.16	0.30
St2	4558-0054	13.01	0.53	−0.12	0.18	0.33
St3	4558-0448	13.93	0.60	0.07	0.48	0.56
St4	4558-0340	14.35	0.39	−0.03	0.33	0.46
St5	4558-0500	14.09	0.43	−0.02	0.32	0.37
St6	4558-2326	15.58	0.99	0.42	1.29	0.82
	NSVS 8626028					
Var	2190-2019	14.23	0.66	0.69	2.07	0.77
St1	2190-1524	10.06	0.40	0.17	1.05	0.27
St2	2190-1134	12.42	0.50	0.27	1.23	0.32
St3	2190-1456	12.76	0.51	0.28	1.26	0.35
St4	2190-0565	12.49	1.12	0.82	2.59	1.09
St5	2190-2044	11.70	1.08	0.54	1.79	0.69

⋆ Standard stars used for the observations with the 2-m telescope.

Table A2. Rozhen photometric data. This is a sample of the full table, which is available with the online version of the article (see Supporting Information). The number of the target is the same as in Table 1.

Target	Filter	*HJD* [d]	Magnitude [mag]	Error [mag]
1	*V*	2455252.267213	12.8632	0.0059
1	*I*	2455252.269054	11.6127	0.0054
1	*V*	2455252.270188	12.8297	0.0059
1	*I*	2455252.272028	11.5911	0.0053
...	...	...	...	...
2	*R*	2455104.580844	14.5421	0.0175
2	*R*	2455104.582256	14.5606	0.0177
2	*R*	2455104.583680	14.5489	0.0177
2	*R*	2455104.585104	14.5417	0.0178
...	...	...	...	...

Table A3. Times of the observed eclipse minima.

HJD(Min) [d]	Filter	Type of minimum	Epoch	$O-C$ [d]
	NSVS 4484038			
2455539.479830	V	Min I	0	0.000563
2455539.479669	I	Min I	0	−0.000174
2455539.589299	V	Min II	0	0.001572
2455539.589183	I	Min II	0	0.001041
2455570.287555	V	Min I	141	−0.001048
2455570.287666	I	Min I	141	−0.000540
2455570.397084	V	Min II	141	0.000236
2455570.397060	I	Min II	141	0.000126
	NSVS 7179685			
2455104.632827	R	Min II	0	−0.003361
2455105.472144	R	Min II	4	−0.001659
2455105.576676	R	Min I	5	−0.003271
2455128.544335	V	Min II	114	0.002112
2455128.543839	R	Min II	114	−0.000253
2455128.543751	I	Min II	114	−0.000672
2455128.648854	V	Min I	115	0.000439
2455128.648414	R	Min I	115	−0.001659
2455128.648348	I	Min I	115	−0.001974
2455262.463012	R	Min I	753	0.000620
2455268.335791	I	Min I	781	0.000901
2455268.440937	I	Min II	781	0.002217
2455563.545264	V	Min II	2188	0.002918
2455563.649773	V	Min I	2189	0.001197
	NSVS 4761821			
2455563.547579	V	Min II	0	0.000365
2455563.546281	I	Min II	0	−0.005603
2455563.656336	V	Min I	1	0.000367
2455563.656667	I	Min I	1	0.001889
2455568.441653	V	Min I	23	0.000509
2455568.441644	I	Min I	23	0.000468
2455568.550426	V	Min II	23	0.000585
2455568.550388	I	Min II	23	0.000411
	NSVS 2700153			
2455368.313740	V	Min I	0	0.006631
2455368.313195	I	Min I	0	0.004246
2455368.425320	V	Min II	0	−0.004959
2455368.426162	I	Min II	0	−0.001274
2455579.518952	V	Min II	924	−0.003699
2455579.518799	I	Min II	924	−0.004368
2455580.548178	V	Min I	929	0.001440
2455580.660175	V	Min II	929	−0.008325
2455581.575046	I	Min II	933	−0.003743
2455581.690325	I	Min I	934	0.000858
	NSVS 925605			
2454988.467268	R	Min II	−1	0.004147
2454989.443816	R	Min I	4	−0.008639
2454989.555544	R	Min II	4	0.004749
2455040.368512	V	Min I	238	−0.010890
2455070.297199	V	Min II	375	0.010704
2455070.296609	R	Min II	375	0.007993
2455070.296099	I	Min II	375	0.005650
2455070.402749	V	Min I	376	−0.004296
2455070.402535	R	Min I	376	−0.005280
2455070.402487	I	Min I	376	−0.005500
2455071.272856	V	Min I	380	−0.006176

Table A3 – *continued*.

HJD(Min) [d]	Filter	Type of minimum	Epoch	$O-C$ [d]
2455071.272715	R	Min I	380	– 0.006824
2455071.272511	I	Min I	380	– 0.007761
2455071.385397	V	Min II	380	0.010948
2455071.384643	R	Min II	380	0.007483
2455071.383811	I	Min II	380	0.003660
		NSVS 8626028		
2455070.516938	V	Min I	0	– 0.000789
2455070.516287	R	Min I	0	– 0.003783
2455070.516218	I	Min I	0	– 0.004101
2455071.496252	V	Min I	5	0.003730
2455071.496096	R	Min I	5	0.003013
2455071.496085	I	Min I	5	0.002962
2455071.604069	V	Min II	5	– 0.000347
2455071.603989	R	Min II	5	– 0.000715
2455071.604153	I	Min II	5	0.000039

SUPPORTING INFORMATION

Additional Supporting Information may be found in the online version of this article:

Table A2. It contains Rozhen photometric observations of the targets. Its columns are: Number of target, filter, HJD, Magnitude, Error (http://mnras.oxfordjournals.org/lookup/suppl/doi:10.1093/mnras/stv147/-/DC1).

Please note: Oxford University Press are not responsible for the content or functionality of any supporting materials supplied by the authors. Any queries (other than missing material) should be directed to the corresponding author for the article.

This paper has been typeset from a TEX/LATEX file prepared by the author.